

DRAFT IPC2020-9787

Time Dependence of Hydrogen Induced Cracking of X70 Pipeline Steel under Severe and Mild Sour Service Conditions using Ultrasonic Analysis

S. Gawor, J.B. Wiskel, D.G. Ivey, J. Liu and H. Henein

Department of Chemical and Materials Engineering
University of Alberta
Edmonton, Alberta, Canada T6G 1H9

ABSTRACT

A standard NACE hydrogen induced crack test was used to evaluate the resistance of two compositions of X70 steel (X70-X (Ca/S ratio of 2.5) and X70-B (Ca/S ratio of <0.5)) under severe (pH = 2.7 and 100% H₂S) and mild (pH = 5.5 and 100% H₂S) sour service conditions. An ultrasonic technique was developed to quantify the severity of hydrogen cracking in both steels as a function of test conditions, steel type and time. In this procedure, a series of local ultrasonic measurements was taken for each test sample to determine a local crack to backwall signal ratio (LCBR). The LCBR values were integrated over the entire sample to give a global crack to backwall ratio (GCBR). A larger GCBR value corresponds to greater hydrogen cracking severity in the sample. Energy dispersive X-ray (EDX) spectroscopy and glancing angle X-ray diffraction (XRD) were used to characterize the surface corrosion products that formed during testing. For severe sour service conditions, the GCBR value reached an asymptotic value of approximately 33% and 47% for X70-X (after 4 days) and X70-B (after 2 days) steels, respectively. For mild sour service conditions, no cracking was observed for testing of less than 16 days. After 32 days, X70-B showed a GCBR of approximately 18%. The onset of cracking of X70-X steel occurred between 32 and 64 days. Samples tested for 64 days showed a GCBR of 30% and 16% for X70-X and X70-B, respectively.

Glancing XRD measurements showed the presence of surface FeS on both steels tested under mild sour service. Quantitative XRD (QXRD) analysis was used to obtain the surface coverage of FeS as a function of test time. EDX mapping confirmed the presence of a high sulfur content over a significant fraction of the surface. XRD measurements of X70-B steel under severe sour service after 8 days did not show a significant amount of FeS. The surface FeS is believed to alter hydrogen ingress into the steel, making it difficult to directly compare

measured GCBR values obtained under mild and severe sour service.

INTRODUCTION

A NACE (TM0284-2016) hydrogen-induced crack (HIC) test is commonly used to assess a steel's susceptibility to cracking under sour service conditions [1]. In this test, sample(s) are exposed to an acidic solution (pH < 7) in which H₂S gas is introduced. The advantages of this test are its relative simplicity and expedient results. Following testing, the HIC sample is sectioned at three (3) locations along its length and the magnitude of cracking is assessed based on direct measurement of the cracks (if any) present on the cut surfaces. The disadvantages of this technique include (but are not limited to) the following: sample sectioning and preparation are time consuming processes (particularly for a large number of HIC samples) and there is an inherent assumption that the sectioned portions of the sample are representative of cracking in the material as a whole. For severe sour service testing conditions (100% H₂S and a pH = 2.7), where extensive HIC cracking is typically observed, the latter limitation may be minimal. However, for HIC tests that are conducted outside the severe sour service regime (e.g., mild sour service with pH = 5.5), and which may be more representative of actual exposure conditions for the steel, less severe cracking during testing is expected. Hence, the ability to observe, and ultimately measure both the onset and magnitude of cracking, requires analysis of the entire sample.

The NACE standard (TM0284-2016) for HIC testing includes a provision for using ultrasonic testing (UT) to detect the presence of cracks in HIC samples. However, the technique is based on binary Yes/No cracking and not on the overall severity of cracking, which would be obtained from standard metallographic analysis of HIC samples and provide a better measure of performance.

Under non severe sour service conditions, the development of corrosion products on the HIC test sample can occur and they may affect the ingress of hydrogen into the sample and ultimately the magnitude of cracking observed. To the knowledge of the author, there is a lack of understanding on how the film affects cracking in mild sour environments with respect to the exposure time.

HIC testing of two X70 steels (with different Ca/S ratios) under severe (pH = 2.7) and mild (pH = 5.5) sour service conditions was undertaken. Following HIC testing, the samples were analyzed by an UT technique developed for this work to quantify the severity of local cracking. Cracking severity maps were plotted, and regions of potential crack initiation and/or high cracking intensity were visually observed. The local severity of cracking measured with UT was validated using optical microscopy. The local cracking measurement was integrated over the entire sample and a global cracking parameter determined. The value of this global cracking parameter was used to compare the HIC resistance of the two types of X70 steels tested under both severe and mild sour service conditions. In addition, scanning electron microscopy coupled with energy dispersive X-ray spectroscopy (SEM/EDX), glancing angle X-ray diffraction (XRD) and quantitative XRD (QXRD) were used to quantify the amount of surface corrosion product(s) that developed with time under mild sour service conditions.

BACKGROUND

A number of studies have been published on HIC testing of pipeline steels, the effect of the Ca/S ratio on HIC cracking resistance, the development of corrosion products on HIC samples and the usage of UT to quantify cracking in HIC samples. This section will review the literature on these topics.

HIC testing of X Grade Steel

HIC testing has been performed on a variety of pipeline steels, such as X65 [2-4], X70 [5], X100 [6] and X120 [7]. The consensus of the research is that hard and brittle microstructures, such as martensite [7] as well as elongated manganese sulfide inclusions [6, 8], greatly increase the susceptibility to hydrogen-induced cracking. Research has shown that the presence of acicular ferrite, acting as a reversible hydrogen trap site, can be linked to increased resistance to hydrogen-induced cracking [2, 5, 9].

Effect of the Ca/S ratio on HIC resistance

Manganese is added to steel to prevent the formation of iron sulfide. However, during the hot rolling process, manganese sulfides are deformed into elongated inclusions [10]. These elongated inclusions are initiation sites for hydrogen-induced cracking [6, 11]. Although modified cross rolling techniques can be used to control the shape of the inclusions, the most effective way to prevent their formation is to modify the chemistry of the steel itself primarily by reducing S content and/or by utilizing Ca for inclusion shape control [10].

Calcium is commonly used for sulfide shape control via the formation of a complex (Mn, Ca, S) inclusions. Ushijima et al. [12] has shown that a Ca/S ratio greater than 2.0 is necessary to promote spherical/globular (Mn, Ca, S) inclusions. Wilson [13] observed that steels treated using sufficient calcium have only slightly deformed/elongated inclusions after hot rolling.

Development of Corrosion Products on HIC Samples

During the hydrogen sulfide corrosion process, polymorphous iron sulfides (e.g., FeS) can be formed [14, 15]. According to Ning et al. [16], sulfide formation depends on the ambient temperature, pH level, exposure time and electrochemical stability of prevalent phases. The initial corrosion product that can occur during HIC testing is believed to be Mackinawite, a metastable iron sulfide, which is formed from the conversion of amorphous or cubic iron sulfide. In addition, Ning et al. have shown that a pH greater than ~4.5 is necessary for the formation of Mackinawite at the surface.

It is widely believed that the formation of an iron and sulfur rich corrosion film significantly increases the protection of the underlying metal and acts to block hydrogen permeation [17, 18]. The film is also believed to suppress the formation of hydrogen atoms. However, Monnot et al. [19] observed the presence of hydrogen within the corrosion film and postulated that the FeS film, for pH levels <4, can act as a reservoir for hydrogen and sustain the absorption of hydrogen into the steel.

Ultrasonic Testing of HIC samples

Ultrasonic techniques have long been used to evaluate different types of hydrogen damage. Szilard and Haynes [20] used ultrasonic shear waves to determine hydrogen embrittlement damage in steel. A change in ultrasonic velocity was observed as a result of increased stress induced by the presence of hydrogen in the steel matrix. Revie et al. [21] used a C-scan technique to analyze the cracking behavior of various steels tested at pH levels ranging from 1.1 to 5.9. Krüger et al. [22] used spectral analysis techniques to detect minute cracks in steel exposed to a NACE TM0177 compliant test solution. Kittel et al. [3, 4] generated ultrasonic maps of X65 HIC test samples and calculated the crack to area ratio (CAR) as a means of comparing the susceptibility of the steel to different pH levels and testing times. After a certain testing time, cracking appears to be stagnant. Further testing does not increase the amount of cracking found in the samples.

EXPERIMENTAL PROCEDURE

X70 steels

Table 1 shows the manganese, sulfur and calcium compositions for the two types of X70 steels, denoted as X70-X and X70-B, as well as the calcium to sulfur ratios. The manganese and calcium amounts are similar in each steel, while the sulfur concentration is ~6 times higher in X70-B. The Ca/S ratio for X70-X and X70-B are 2.5 and <0.5, respectively. In this

paper, reference to X70-B will infer either X70-B (1) or X70-B (2) interchangeably.

Table 1 – Mn, S and Ca Compositions of X70-X and X70-B

Sample	Mn (wt %)	S (wt %)	Ca (wt %)	Ca/S
X70-X	1.59	0.001	0.0025	2.5
X70-B (1)	1.62	0.0057	0.0022	0.386
X70-B (2)	1.59	0.0057	0.0025	0.439

HIC Testing

The HIC test conditions, including solution pH and test duration, are shown in Table 2. For each condition one sample was tested using the standard NACE TM0284 test procedure [1] and 100% H₂S gas. Test samples, analyzed using glancing angle XRD to characterize surface scale, are noted in the table.

Table 2 – HIC test conditions

Sample	pH	Time (days)	XRD Analysis
X70-X	2.7	1, 2, 4, 8, 16	8 days only
X70-X	5.5	1, 2, 8, 16, 32, 64	-
X70-B	2.7	1, 2, 8, 16	-
X70-B	5.5	1, 2, 8, 16, 32, 64	All

UT Analysis

Following HIC testing, the samples were cleaned using acetone and ethanol and a 5 mm x 5 mm square grid was applied to the surface of the HIC sample as shown in Figure 1a. The 5 mm grid (shown in plane view in Figure 1b) corresponds to the diameter of the 5 mm longitudinal ultrasonic probe (Olympus V203-RM) used. The ultrasonic probe was connected to a data acquisition board and each UT scan was downloaded to a computer for subsequent analysis. In total, eighty (80) ultrasonic scans were taken for each HIC sample.

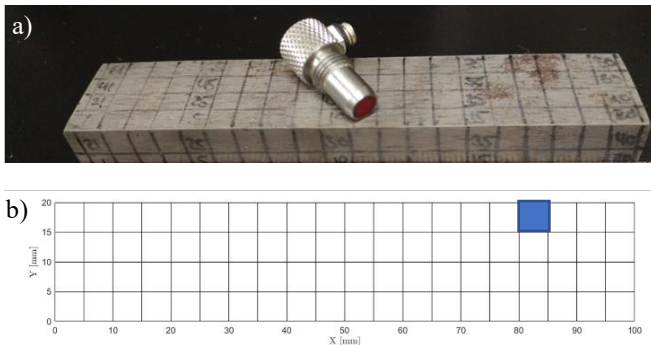


Figure 1 – a) HIC sample with grid applied and b) schematic of grid in plane view.

An example of an ultrasonic scan (intensity vs. time) is shown in Figure 2 (location 77, highlighted in Figure 1b). Each peak on the scan, corresponding to a reflection of the UT signal from either a crack signal (assumed to occur at the centreline) or combined crack and backwall signal, was detected based on the envelope function (localized spline interpolation to determine actual UT peaks location) of the raw ultrasonic data. The combined backwall and crack signal intensity (designated by a filled circle) was fit to an exponential time function (analogous to a UT attenuation equation). A local crack to backwall ratio (LCBR) ratio was then calculated using the following equation:

$$LCBR = \frac{I_c}{(I_c' + I_b')} \cdot 100\%$$

where I_c is the first measured crack signal intensity and $I_c' + I_b'$ represents the predicted (from the fitted curve) combined crack and backwall signal intensity calculated at the crack signal time.

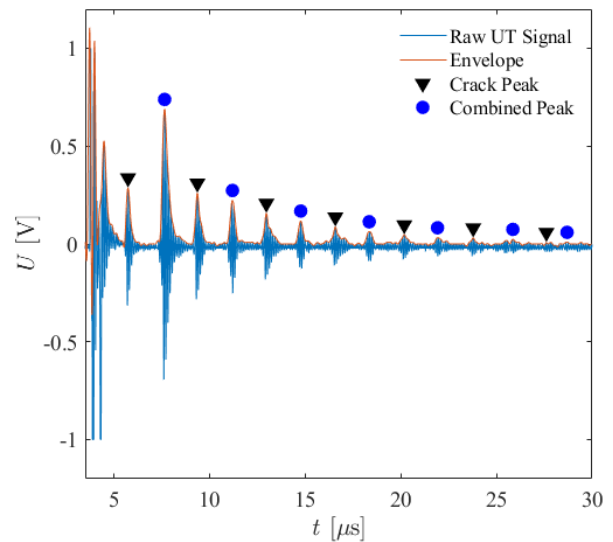


Figure 2 – Measured ultrasonic data for X70-X (pH 2.7, 8 days) taken at grid location 77 in Figure 1b.

This procedure was repeated for each grid scan. Figure 3 shows the complete LCBR map for X70-X (pH 2.7, 8 days). In this map, the LCBR values for each individual grid location are represented in a 32-tone grey scale (Fig. 4), where entirely white cells have an LCBR of 0% (no cracking) and black cells have an LCBR of 100% (the crack covers the entire individual grid). The grey tones between the two extremes indicate different severities of cracking at each grid point.

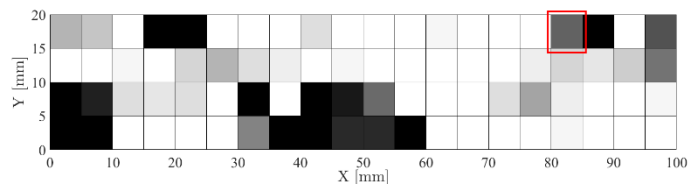


Figure 3 – LCBR map for X70-X, tested in pH 2.7 for 8 days; the red box marks location 77 in Figure 1b.



Figure 4 – Visualization of 32-tone grey scale used for LCBR.

Global Crack to Backwall Ratio

The global crack to backwall ratio (GCBR) was calculated from all LCBR ratios using the following equation:

$$\text{GCBR} = \frac{\sum_{i=1}^n \text{LCBR}(i)}{n}$$

where n represents the number of grid points. This value was determined for each HIC test and was used to compare the HIC susceptibility of each steel under different test conditions. The GCBR represents the overall cracking in an entire HIC bar.

Column-wise Crack to Backwall Ratio

To compare ultrasonic data, such as CBR, to the NACE TM0284-2016 sectioning results, an additional ratio is defined. This ratio, the column-wise crack to backwall signal ratio (CCBR), is used to quantify cracking in a single column of the test grid (i.e., 4 vertically adjacent data sets). The CCBR was calculated using the following equation:

$$\text{CCBR} = \frac{\sum_{i=1}^4 \text{LCBR}(i + (i - 1) \cdot 20)}{4}$$

where i represents the column of interest.

Validation of Ultrasonic Methodology

The NACE TM0284-2016 sectioning method was used for validation of the ultrasonic results. X70-B, tested for 32 days at a pH of 5.5, was sectioned into 25 mm slices, at locations 25 mm (A), 50 mm (B) and 75 mm (C). Figure 5 shows the corresponding GCBR map, as well as the location of the three slices (A, B and C). The sectioned surfaces were then mounted and polished, using 0.05 μm diamond paste as the final polish. To enhance crack visibility, the samples were etched with 2% Nital. The etched surface was examined at 100X magnification and the length and width of each crack was recorded. Based on the crack dimensions found, the crack to length ratio (CLR), crack to thickness ratio (CTR) and crack sensitivity ratio (CSR) were calculated using the following equations:

$$\text{CLR} = \frac{\sum L_c}{L_s}$$

$$\text{CTR} = \frac{\sum T_c}{T_s}$$

$$\text{CSR} = \frac{\sum (L_c \cdot T_c)}{L_s \cdot T_s}$$

where L_s and T_s represent the length and thickness, respectively, of the test specimen and L_c and T_c are the length and thickness, respectively, of the cracks.

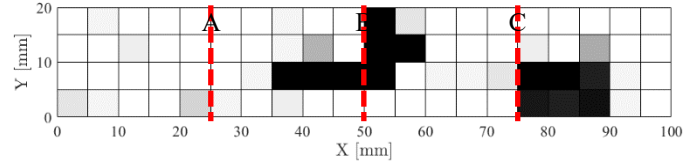


Figure 5 – LCBR map for X70-B, tested at pH 5.5 for 32 days, showing the OM analysis sectioning locations (A, B and C).

Glancing Angle XRD and SEM/EDX

Glancing angle XRD patterns were obtained for X70-B samples tested for 1-32 days at a pH of 5.5. All samples were cut along the normal and rolling direction of the steel and cleaned in acetone and ethanol. Each sample has a dimension of approximately 7x7 mm with a thickness of approximately 2 mm. The angular increment was 2 degrees/s and the copper (Cu K- α) radiation wavelength was 1.5406 \AA . The normalized XRD pattern for X70-B for a pH of 5.5 and 32 days is shown in Figure 6. Included are markers indicating the FeS (Mackinawite) diffraction peaks.

All samples tested using XRD were verified using SEM and EDX and images were taken at 100x magnification. Rietveld analysis (quantitative XRD) [23] was utilized to determine the amount of Mackinawite at the surface.

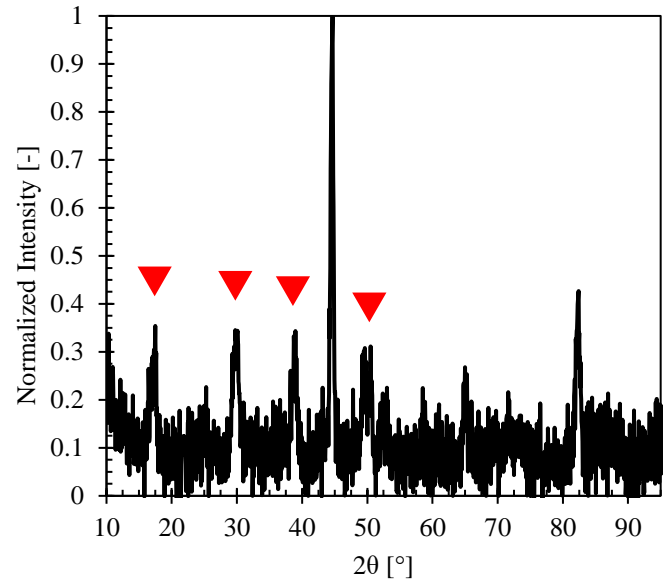


Figure 6 – Normalized XRD pattern for X70-B, tested for 32 days (pH 5.5), with markers indicating FeS (Mackinawite) peaks.

RESULTS AND DISCUSSION

In the following sections, a comparison between the measured LCBR and the optical microscopy analysis of cracking at select locations for X70-B (tested for 32 days at a pH of 5.5) is shown. The global crack to backwall ratio (GCBR) for each HIC test is calculated and used to compare the susceptibility of the two X70 steels to hydrogen cracking. Surface analysis of the mild service conditions using QXRD and SEM/EDX is also presented.

Comparison of ultrasonic LCBR and cracking measured using optical microscopy

The average (column wise) CCBR on either side of the sample sectioning location (left or right) for the X70-B sample (pH = 5.5 and 32 days) was determined. These values are shown in Table 3 for the 25, 50 and 75 mm sectioning locations (Figure 5). Included in Tables 3 and 4 are the values of total crack length and width, as well as CLR, CTR and CSR calculated from the optical microscope image at each section location.

Table 3 – Measured crack lengths for X70-B after 32 days (pH 5.5)

Cut Position (mm)	Crack Length (μm)	Crack Width (μm)
25	174	61
50	13842	1113
75	592	50

Table 4 – UT and OM crack data at 25, 50 and 75 mm sectioning locations

Cut Position (mm)	CCBR		CLR (%)	CTR (%)	CSR (%)	CCBR Column Right
	Column Left	Column Right				
25	4.7	0.9	1.0	1.0	0	0.9
50	25	75	69	11	8	75
75	3.1	49.6	3	0	0	49.6

The average CCBR was then compared to the CLR. For the 25 mm slice, a CLR of 1% was measured. The corresponding LCBR values were 4.7% and 0.9%. At 50 mm, a CLR of 69% was measured and the CCBR values are 25% and 75%. For 75 mm, a CLR of 3% was determined, with corresponding CCBR values of 3.1% and 49.6%. Overall, the optical method (based on sectioning) and the ultrasonic method show similar HIC cracking intensity values, such that a low CLR (1.0%) corresponds to a low CCBR (4.7 and 0.9%) and a high CLR (69%) corresponds to a high CCBR (25 and 75%).

For the 75 mm slice, the low CLR (3%) only agrees with the left side CCBR value (3.1%). This value is quite different from the very high CCBR (49.6%) immediately right of the OM cut.

This suggests that unlike UT analysis, small differences in OM sectioning can lead to an erroneous representation of the actual amount of cracking.

GCBR Testing Results at pH 2.7

HIC samples were analyzed using the developed CBR technique. For the tests carried out at pH 2.7 (Figure 7), the onset of cracking for X70-X and X70-B appears to be identical. After two days, the cracking observed in X70-X is significantly less than that observed in X70-B (GCBR ~13% vs. ~47% (averaged over two data points from two different samples)). Both X70-X and X70-B show cracking plateaus between 4-16 and 2-16 days, respectively. The plateau present in the X70-X data set fluctuates around 33% cracking. For X70-B, a 47% cracking plateau is observed.

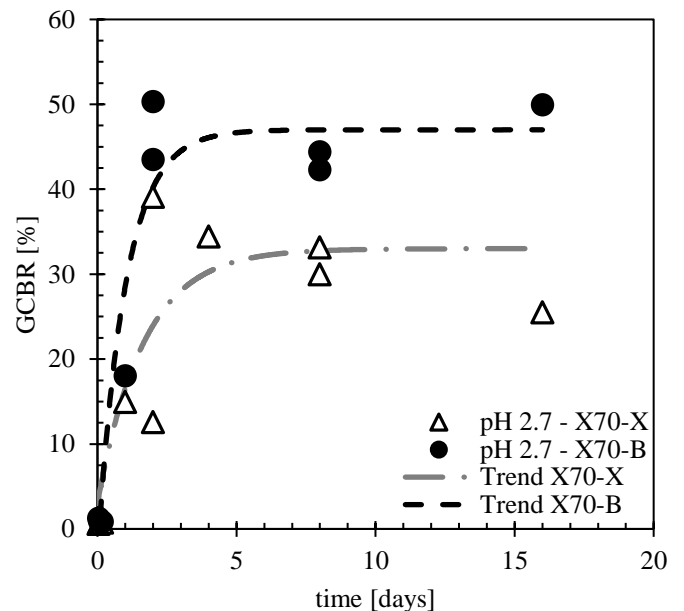


Figure 7 – HIC testing series for pH 2.7.

GCBR Testing Results at pH 5.5

Samples tested at pH 5.5 (Figure 8) show virtually no cracking for testing times of 16 days or less. X70-B had a GCBR of 18% after 32 days in the test solution. X70-X first showed cracking after 64 days in solution. After 64 days, X70-X and X70-B show ~29% and ~16% cracking, respectively. A plateau can be seen for X70-B between 32 and 64 days. Cracking after this time is ~19%.

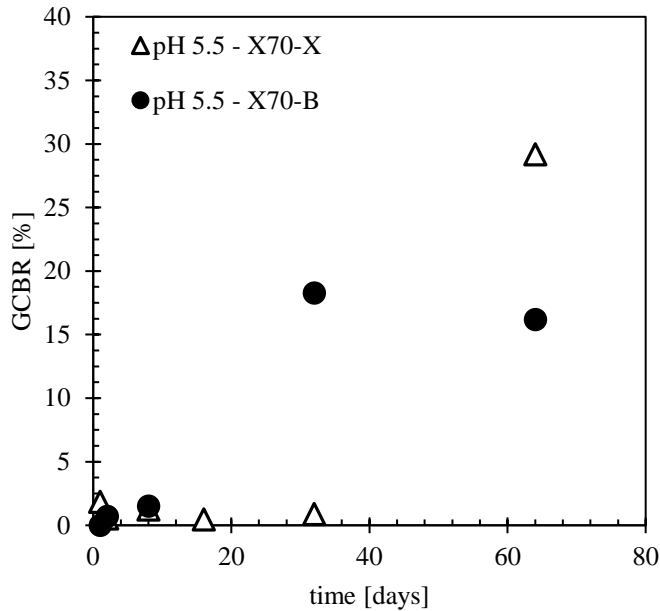


Figure 8 – HIC testing series for pH 5.5.

Surface Cracking of HIC samples

One possible explanation for the presence of crack plateaus may be related to surface cracking observed for the HIC test samples. The LCBR map (Figure 9a) for X70-X (pH = 2.7 and 16 days) shows an LCBR of 100% (i.e., complete cracking) at a number of edge locations. Figure 9b shows a 7.5 mm long edge crack observed in the sample at the 65-75 mm location. An additional surface crack was observed between 25 and 45 mm. The presence of these surface cracks may allow internal hydrogen to escape and prevent a critical pressure for crack initiation inside the steel, effectively limiting further cracking.

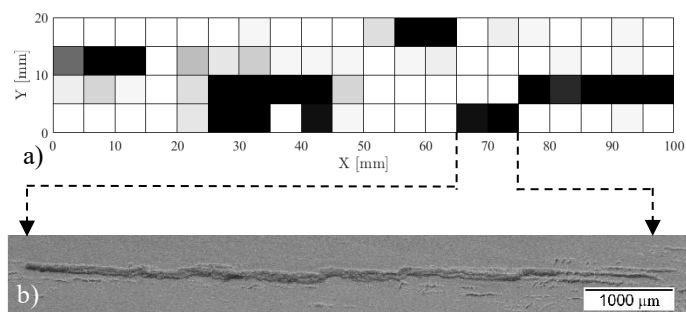


Figure 9 – (a) LCBR map for X70-X after 16 days of testing at pH 2.7 and (b) surface crack observed at the location between 65 and 75 mm (b).

Analysis of Surface Scale

Increasing discoloration with testing time was observed for samples tested at pH 5.5. This discoloration can be associated with the formation of FeS in its Mackinawite state. Using

glancing angle QXRD and Rietveld refinement, the external corroded surface was examined. The amount of Mackinawite at the surface (wt.%) was determined for X70-B for samples tested for 1 to 64 days. Using the specific gravities for iron [24] and Mackinawite [25], a volume fraction for FeS was calculated. By assuming an X-ray penetration depth of 2 μm, the volume fraction was converted into an area percent (Figure 10).

A rapid increase in the area fraction FeS occurs between 1-2 and 8 days of testing time. At the time during which cracking was first observed (32 days), ~86% of the surface was covered with FeS. Samples tested for 64 days have about the same surface coverage (~83%). These results indicate that the onset of HIC cracking under conditions of mild sour service, in conjunction with the development of a surface corrosion product, is complicated. If the corrosion film acts as a barrier to hydrogen ingress, as detailed earlier [17,18], then the continual formation of the FeS film delays HIC cracking. Conversely, if the corrosion film acts as a reservoir for hydrogen [18], then the onset of cracking after 32 days (maximum amount of FeS) could be explainable by this phenomenon. Assuming that the pH distribution within the test solution is homogenous, no hydrogen reservoirs should be expected in the corrosion film. However, if the pH decreases to <4 locally, hydrogen could accumulate in the scale. This would result in a localized, but temporary source of hydrogen and could result in the initiation of localized surface cracks.

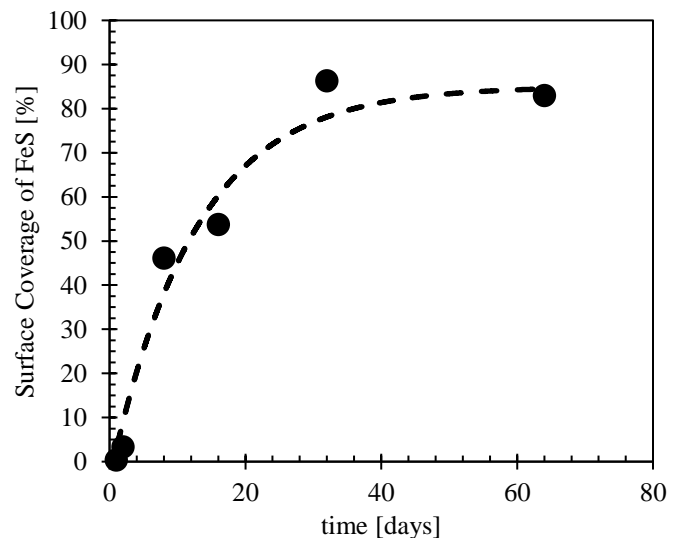


Figure 10 – Surface area coverage of FeS (Mackinawite) as a function of time for X70-B tested under mild sour service conditions (pH 5.5).

Figure 11 and 12 show the progression in surface morphology for 1 (Figure 11) and 32 days (Figure 12), respectively. The horizontal banding, most prominent in Figure 11, shows the residual grinding marks from the processing of the HIC bars. For testing times of 8 days and less, the banding on the surface is mostly even, but is starting to show pitting corrosion. Both EDX analysis and glancing angle XRD confirm that the

change in banding is related to the formation of FeS (Mackinawite). After 32 days in testing solution, X70-B shows significant growth of the FeS film on the steel surface, covering most of the surface.

Figure 13 and 14 show the EDX map for sulfur for the areas shown in Figure 11 and 12, respectively. The map for the 1-day test shows traces of sulfur along the banding (Figure 13). In direct comparison, the EDX map for sulfur for the 32-day test (Figure 14) shows significantly more sulfur on the surface. These results correlate well with the results obtained from the Rietveld refinement.

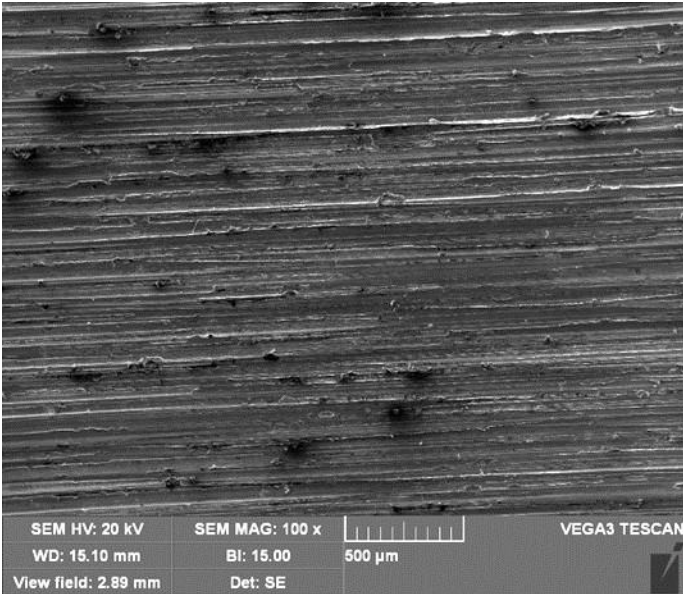


Figure 11 – SEM image of surface morphology for X70-B, tested at pH 5.5, after 1 day.

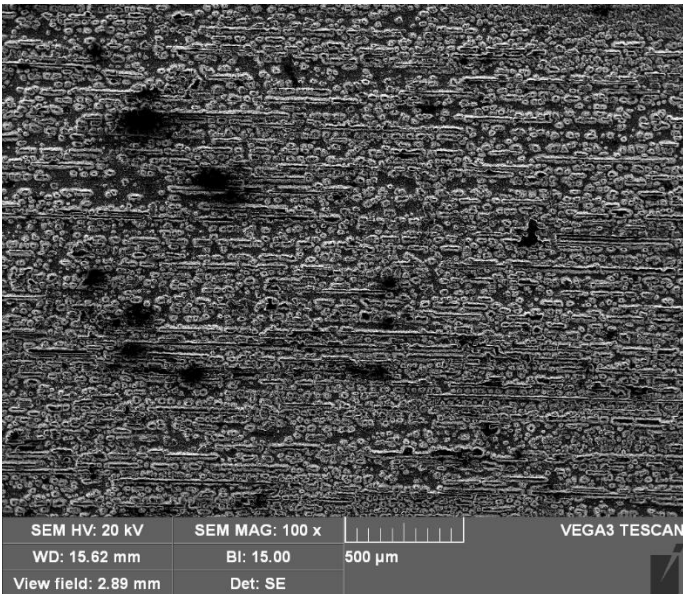


Figure 12 – SEM image of surface morphology for X70-B, tested at pH 5.5, after 32 days.

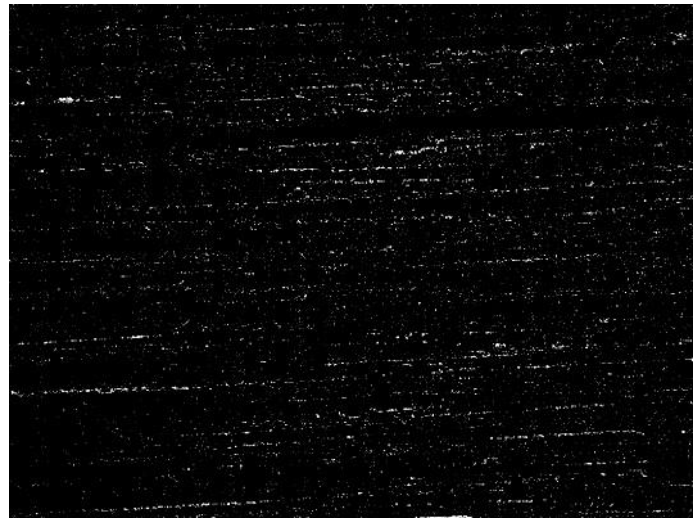


Figure 13 – EDX map of sulfur for X70-B, tested at pH 5.5, after 1 day.

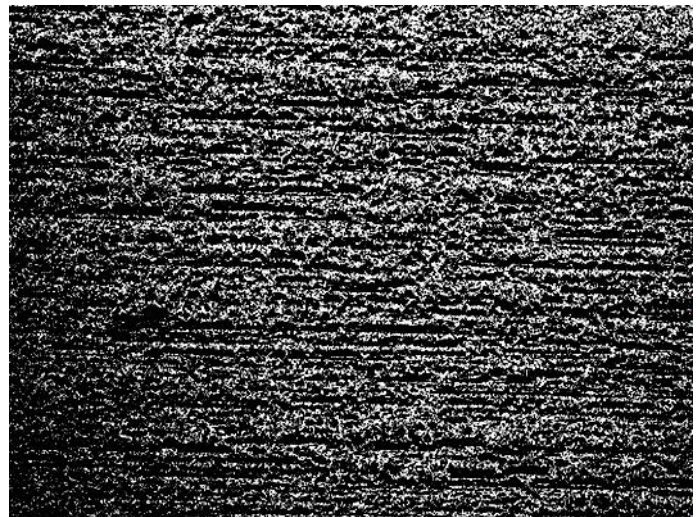


Figure 14 – EDX map of sulfur for X70-B, tested at pH 5.5, after 32 days.

Figure 15 shows a 750x magnification SEM image of X70-B after 32-days HIC testing (pH =5.5). An EDX map for sulfur of the area shown in Figure 15 is presented in Figure 16. It can be seen that sulfur is present in intermittent clusters and does not cover the whole steel surface homogeneously. This agrees with the surface coverage shown in Figure 10.

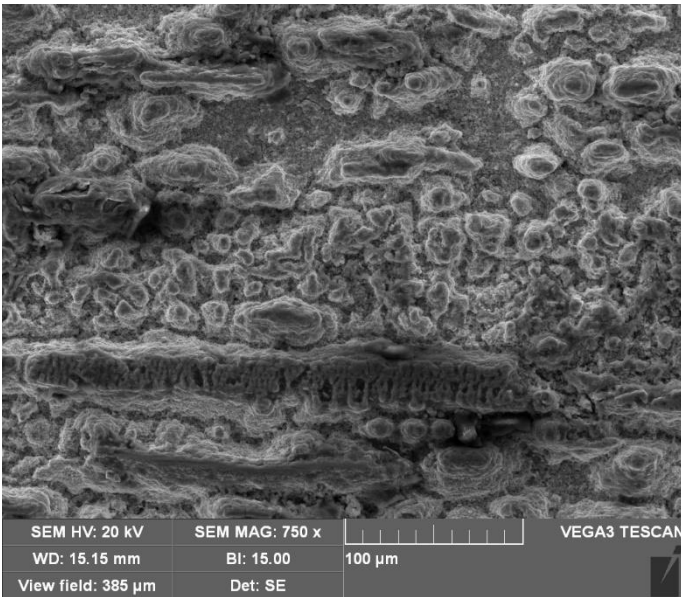


Figure 15 – SEM image of surface morphology for X70-B, tested at pH 5.5, after 32 days.

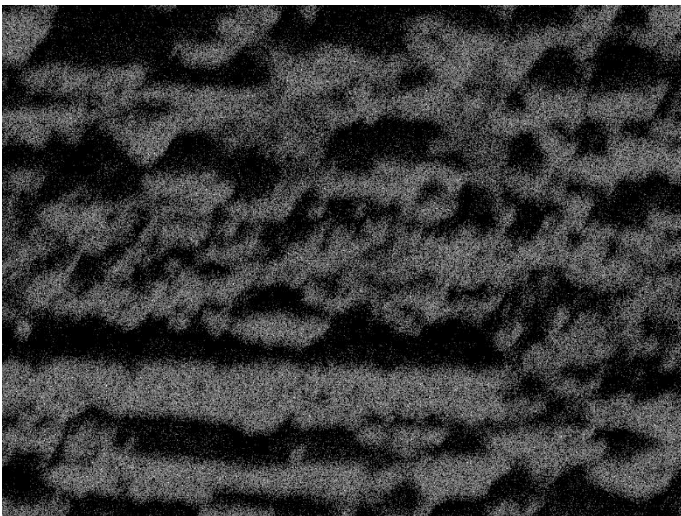


Figure 16 – EDX map of sulfur for X70-B, tested at pH 5.5, after 32 days (750x magnification).

CONCLUSIONS

A novel methodology for the measurement and quantification of cracking during HIC testing was developed. This technique has been applied to two X70 steels with different Ca/S ratios (X70-X: Ca/S = 2.5 and X70-B: Ca/S < 0.5) and tested under severe (pH = 2.7) and mild sour (pH = 5.5) service conditions. The ease of evaluation of HIC cracking using this technique and the unique information it provides can be readily applied to HIC testing of a variety of sour service material with different microstructures and under different sour service conditions. Using this new technique, the following conclusions can be drawn:

1] For severe sour service conditions (pH = 2.7), samples with a Ca/S ratio of <0.5 (X70-B) showed significantly more cracking compared to those with a Ca/S ratio of 2.5 (X70-X). Crack formation reaches a plateau after 2-4 days of testing.

2] A delayed onset of cracking was observed for samples tested under mild sour service conditions (pH = 5.5). No cracking was observed for testing times of 16 days or less for X70-X or X70-B. X70-B first showed cracking after 32 days. The amount of cracking observed after 64 days was almost identical to that observed after 32 days. X70-X exclusively showed cracking after 64 days. The global crack to backwall signal ratio (GCBR) obtained for this test was approximately 50% higher than that of X70-B.

3] The use of the conventional NACE TM0284 sectioning method has proven to be more time consuming and less accurate than the proposed ultrasonic method. As a result of limiting the analysis to 3 (three) cut surfaces (25 mm apart), potentially non-representative sample areas are analyzed and inaccurate conclusions with respect to the magnitude of cracking behaviour may be drawn, particularly for mild sour service testing (pH = 5.5) where extensive cracking is not observed.

4] Surface cracking was observed visually and corresponded to high local crack to backwall signal ratios (LCBR). These surface cracks could allow internal hydrogen to escape from the steel and prevent critical hydrogen pressure buildup; hence, limiting the overall magnitude of cracking.

5] XRD analysis of samples tested under mild sour service conditions (pH = 5.5) for 1-64 days showed the formation of FeS (Mackinawite) scale. The amount of corrosion scale increased with testing duration and reached a plateau at 32 days.

NOMENCLATURE

CAR	Crack to Area Ratio
CBR	Crack to Backwall Signal Ratio
CCBR	Column-wise Crack to Backwall Signal Ratio
CLR	Crack to Length Ratio
CSR	Crack Sensitivity Ratio
CTR	Crack to Thickness Ratio
EDX	Energy Dispersive Spectroscopy
GCBR	Global Crack to Backwall Signal Ratio
HIC	Hydrogen-Induced Cracking
LCBR	Local Crack to Backwall Signal Ratio
OM	Optical Microscopy
XRD	X-Ray Diffraction
UT	Ultrasonic Testing

ACKNOWLEDGMENTS

The authors would like to thank Laurie Collins, Tirdad Nickchi and EVRAZ N.A. Inc for valuable input and financial support, Robert Lazor and TC Energy for samples and financial support and NSERC for financial support.

REFERENCES

1. NACE, "NACE TM0284-2016 - Evaluation of pipeline and pressure vessel steels for resistance to hydrogen-induced cracking," 2016.
2. A.V. Latifi, R. Miresmaeili and A. Abdollah-Zadeh, "The mutual effects of hydrogen and microstructure on hardness and impact energy of SMA welds in X65 steel," *Materials Science and Engineering: A*, vol. 679, pp. 87–94, 2017.
3. J. Kittel, V. Smanio, M. Fregonese, L. Garnier, and X. Lefebvre, "Hydrogen induced cracking (HIC) testing of low alloy steel in sour environment: Impact of time of exposure on the extent of damage," *Corrosion Science*, vol. 52, no. 4, pp. 1386 – 1392, 2010.
4. J. Kittel, J. W. Martin, and T. Cassagne, "Hydrogen induced cracking (HIC) – laboratory testing assessment of low alloy steel linepipe," *Corrosion NACE-08110*, 2008.
5. B. Beidokhti, A. Dolati and A.H. Koukabi, "Effects of alloying elements and microstructure on the susceptibility of the welded HSLA steel to hydrogen-induced cracking and sulfide stress cracking," *Materials Science and Engineering: A*, vol. 507, pp. 167–173, 2009.
6. L. Gan, F. Huang, X. Zhao, J. Liu and F. Cheng, "Hydrogen trapping and hydrogen induced cracking of welded X100 pipeline steel in H₂S environments," *International Journal of Hydrogen Energy*, vol. 43, pp. 2293–2206, 2018.
7. F. Huang, J. Liu, Z. Deng, J. Cheng, Z. Lu, and X. Li, "Effect of microstructure and inclusions on hydrogen induced cracking susceptibility and hydrogen trapping efficiency of X120 pipeline steel," *Material Science and Engineering: A*, vol. 527, pp. 6997–7001, 2010.
8. X. Du, W. Cao, C. Wang, S. Li, J. Zhao, and Y. Sun, "Effect of microstructures and inclusions on hydrogen-induced cracking and blistering of A537 steel," *Materials Science and Engineering: A*, vol. 642, pp. 181–186, 2015.
9. G.T. Park, S.U. Koh, H.G. Jung and K.Y. Kim, "Effect of microstructure on the hydrogen trapping efficiency and hydrogen induced cracking of linepipe steel," *Corrosion Science*, vol. 50, no. 7, pp. 1865–1871, 2008.
10. L. Luyckx, J. R. Bell, A. McLean, and M. Korchynsky, "Sulfide shape control in high strength low alloy steels," *Metallurgical Transactions*, vol. 1, pp. 3341–3350, 1970.
11. S. Ouhiba, "Hydrogen induced cracking and sulfide stress cracking," Master's thesis, University of Alberta, Edmonton, AB, 2017.
12. K. Ushijima, Y. Sugitani, S. Yamaguchi, S. Shiode, M. Hashio, and H. Tomono, "The technology of continuous casting for the application of HSLA steels," in *Int. Conf. on HSLA Steels, Technology and Application (Materials Park, OH: ASM International, 1984)*, pp. 403–409.
13. A. Wilson, "Characterizing inclusion shape control in low-sulfur C-Mn-Nb steels," *HSLA Steels, Technology and Applications*, pp. 419–427, 1983.
14. P. Taylor, "Stereochemistry of iron sulfides: a structural rationale for the crystallization of some metastable phases from aqueous solution," *Am. Mineral. (United States)*, vol. 65, no. 9, 1980.
15. J. Smith and J. Miller, "Nature of sulphides and their corrosive effect on ferrous metals: a review," *British Corrosion Journal*, vol. 10, no. 3, pp. 136–143, 1975.
16. J. Ning, Y. Zheng, D. Young, B. Brown, and S. Nešić, "Thermodynamic study of hydrogen sulfide corrosion of mild steel," *Corrosion*, vol. 70, no. 4, pp. 375–389, 2013.
17. C. Zhou, S. Zheng, C. Chen and G. Lu, "The effect of the partial pressure of H₂S on the permeation of hydrogen in low carbon pipeline steel," *Corrosion Science*, vol. 67, pp. 184–192, 2013.
18. F. Huang, P. Cheng, X. Y. Zhao, J. Liu, Q. Hu, Y. F. Cheng, "Effect of sulfide films formed on X65 steel surface on hydrogen permeation in H₂S environments," *International Journal of Hydrogen Energy*, vol. 42, pp. 4561–4570, 2017.
19. M. Monnot, R. P. Nogueira, V. Roche, G. Berthomé, E. Chauveau, R. Estevez and M. Mantel, "Sulfide stress corrosion study of a super martensitic stainless steel in H₂S sour environments: Metallic sulfides formation and hydrogen embrittlement," *Applied Surface Science*, vol. 394, pp. 132–141, 2017.
20. J. Szliard and R. Haynes, "Ultrasonic detection of hydrogen embrittlement in steel," in *1978 Ultrasonics Symposium. IEEE*, pp. 316–319, 1978.
21. R. Revie, V. Sastri, G. Hoey, R. Ramsingh, D. Mak, and M. Shehata, "Hydrogen-induced cracking of linepipe steels part 1—threshold hydrogen concentration and pH," *Corrosion*, vol. 49, no. 1, pp. 17–23, 1993.
22. S. Krüger, J. Rebello, and P. De Camargo, "Hydrogen damage detection by ultrasonic spectral analysis," *NDT & E International*, vol. 32, no. 5, pp. 275–281, 1999.
23. J. B. Wiskel, X. Li, D. G. Ivey and H. Henein, "Characterization of X80 and X100 Microalloyed Pipeline Steel Using Quantitative X-ray Diffraction", vol. 49B, pp. 1597-1611, 2018.
24. D. Havel, "Austenitic Manganese Steel - A complete Review", *Columbia Steel Casting Co., Inc*, 2017.
25. A. M. El-Sherik, J. Kvarekvål and J. Moloney, "Trends in Oil and Gas Corrosion Research and Technologies - Production and Transmission", Chapter 6: Sour Corrosion, Woodhead Publishing: Online, p. 119, 2017.